

Electromagnetic surface waves guided by the planar interface of isotropic chiral materials

Maimoona Naheed¹, Muhammad Faryad² and Tom G. Mackay^{3,4,1}

¹*Department of Electronics, Quaid-i-Azam University, Islamabad, Pakistan*

²*Department of Physics, Lahore University of Management Sciences, Lahore, Pakistan*

³*School of Mathematics and Maxwell Institute for Mathematical Sciences,
University of Edinburgh, Edinburgh EH9 3JZ, United Kingdom*

⁴*NanoMM—Nanoengineered Metamaterials Group, Department of Engineering Science and
Mechanics, Pennsylvania State University, University Park, PA 16802–6812, USA*

Abstract

The propagation of electromagnetic surface waves guided by the planar interface of two isotropic chiral materials, namely materials \mathcal{A} and \mathcal{B} , was investigated by numerically solving the associated canonical boundary-value problem. Isotropic chiral material \mathcal{B} was modeled as a homogenized composite material, arising from the homogenization of an isotropic chiral component material and an isotropic achiral, non-magnetic, component material characterized by the relative permittivity $\varepsilon_a^{\mathcal{B}}$. Changes in the nature of the surface waves were explored as the volume fraction $f_a^{\mathcal{B}}$ of the achiral component material varied. Surface waves are supported only for certain ranges of $f_a^{\mathcal{B}}$; within these ranges only one surface wave, characterized by its relative wavenumber q , is supported at each value of $f_a^{\mathcal{B}}$. For $\text{Re}\{\varepsilon_a^{\mathcal{B}}\} > 0$, as $|\text{Im}\{\varepsilon_a^{\mathcal{B}}\}|$ increases surface waves are supported for larger ranges of $f_a^{\mathcal{B}}$ and $|\text{Im}\{q\}|$ for these surface waves increases. For $\text{Re}\{\varepsilon_a^{\mathcal{B}}\} < 0$, as $|\text{Im}\{\varepsilon_a^{\mathcal{B}}\}|$ increases the ranges of $f_a^{\mathcal{B}}$ that support surface-wave propagation are almost unchanged but $|\text{Im}\{q\}|$ for these surface waves decreases. The surface waves supported when $\text{Re}\{\varepsilon_a^{\mathcal{B}}\} < 0$ may be regarded as akin to surface-plasmon-polariton waves, but those supported for when $\text{Re}\{\varepsilon_a^{\mathcal{B}}\} > 0$ may not.

1 Introduction

Electromagnetic surface waves are guided by the planar interface of two dissimilar materials. Various types of electromagnetic surface wave have been identified since the early 1900s right up to the present day. The type assigned to a given surface wave depends upon whether the partnering materials are isotropic or anisotropic, dissipative or nondissipative, homogeneous or nonhomogeneous, etc. [1]. The planar interface of a plasmonic material and a dielectric material guides the surface-plasmon-polariton (SPP) wave [2, 3], which is the most well-known type of electromagnetic surface wave. The partnering materials for SPP waves may be isotropic or anisotropic [4]. Uses for these waves are found in optical sensing [5, 6]. Another well-known

¹Corresponding author. E-mail: T.Mackay@ed.ac.uk

type of electromagnetic surface wave is the Dyakonov wave [7, 8], which is guided by the planar interface of an isotropic dielectric material and an anisotropic dielectric material [9, 10]. Dyakonov waves are generally associated with small angular existence domains [11] but larger angular existence domains can be supported if the partnering materials are dissipative [12, 13]. Surface waves that are intermediate in character, in part akin to SPP waves and in part akin to Dyakonov waves, can be supported by hyperbolic materials [4, 14, 15].

Owing to their inherent magneto-electric coupling, chiral materials [16] offer wider opportunities for surface-wave propagation than achiral materials. To date, there have been relatively few studies of the surface waves supported by chiral materials [17–20], as compared to achiral materials. Most of these studies have concentrated on interfaces of nondissipative chiral materials and isotropic plasmonic materials. The corresponding surface waves in these studies are akin to SPP waves. Recently, surface waves guided by the planar interfaces of chiral materials and anisotropic achiral materials were explored numerically [21]. In this study surface waves akin to Dyakonov waves were found to be supported when the achiral partnering material was a dielectric material while surface waves akin to SPP waves were found to be supported when the achiral partnering material was a plasmonic material.

In the following we consider the previously-unexplored case of surface waves guided by the planar interface of two isotropic chiral materials. The dispersion relation corresponding to the canonical boundary-value problem [1] is derived and numerical solutions are extracted. To allow greater flexibility for our numerical investigations, both isotropic chiral partnering materials are modeled as homogenized composite materials (HCMs) [22]. Furthermore, a novel type of chiral material that can simultaneously support attenuation and amplification of plane waves [23], depending upon circular polarization state, is utilized.

As regards notation, the permittivity and permeability of free space are written as ϵ_0 and μ_0 , respectively. The free-space wavelength is $\lambda_0 = 2\pi/k_0$ with the free-space wavenumber being $k_0 = \omega\sqrt{\epsilon_0\mu_0}$ and ω being the angular frequency. The operators $\text{Re}\{\cdot\}$ and $\text{Im}\{\cdot\}$ deliver the real and imaginary parts of complex-valued quantities, and $i = \sqrt{-1}$. Single underlining signifies a 3 vector and the triad of unit vectors aligned with the Cartesian axes are $\{\hat{\underline{u}}_x, \hat{\underline{u}}_y, \hat{\underline{u}}_z\}$. Matrixes are enclosed by square brackets.

2 Theory: canonical boundary-value problem for surface-wave propagation

Let us consider the canonical boundary-value problem for surface waves [1] guided by the planar interface of two different isotropic chiral materials. Both partnering materials are homogeneous. The isotropic chiral material, labeled \mathcal{A} , fills the half-space $z > 0$ and is characterized by the frequency-domain Tellegen constitutive relations [16]

$$\left. \begin{aligned} \underline{D}(\underline{r}) &= \epsilon_0 \epsilon_{\mathcal{A}} \underline{E}(\underline{r}) + i\sqrt{\epsilon_0\mu_0} \xi_{\mathcal{A}} \underline{H}(\underline{r}) \\ \underline{B}(\underline{r}) &= -i\sqrt{\epsilon_0\mu_0} \xi_{\mathcal{A}} \underline{E}(\underline{r}) + \mu_0 \mu_{\mathcal{A}} \underline{H}(\underline{r}) \end{aligned} \right\}, \quad z > 0, \quad (1)$$

while the isotropic chiral material, labeled \mathcal{B} , fills the half-space $z < 0$ and is characterized by the frequency-domain Tellegen constitutive relations [16]

$$\left. \begin{aligned} \underline{D}(\underline{r}) &= \epsilon_0 \epsilon_{\mathcal{B}} \underline{E}(\underline{r}) + i\sqrt{\epsilon_0\mu_0} \xi_{\mathcal{B}} \underline{H}(\underline{r}) \\ \underline{B}(\underline{r}) &= -i\sqrt{\epsilon_0\mu_0} \xi_{\mathcal{B}} \underline{E}(\underline{r}) + \mu_0 \mu_{\mathcal{B}} \underline{H}(\underline{r}) \end{aligned} \right\}, \quad z < 0. \quad (2)$$

The relative permittivity scalars $\epsilon_{\mathcal{A},\mathcal{B}}$, the relative permeability scalars $\mu_{\mathcal{A},\mathcal{B}}$, and the relative chirality pseudoscalars $\xi_{\mathcal{A},\mathcal{B}}$ are frequency dependent and generally complex valued, per the principle of causality embodied by the Kramers–Kronig relations [24].

The electromagnetic field phasors in the partnering materials \mathcal{A} and \mathcal{B} are represented by

$$\left. \begin{aligned} \underline{E}_{\ell}(\underline{r}) &= \underline{\mathcal{E}}_{\ell} \exp(i\underline{k}_{\ell} \cdot \underline{r}) \\ \underline{H}_{\ell}(\underline{r}) &= \underline{\mathcal{H}}_{\ell} \exp(i\underline{k}_{\ell} \cdot \underline{r}) \end{aligned} \right\}, \quad \ell \in \{\mathcal{A}, \mathcal{B}\}. \quad (3)$$

The amplitude vectors $\underline{\mathcal{E}}_\ell$ and $\underline{\mathcal{H}}_\ell$ have complex-valued components, and so does the wave vector \underline{k}_ℓ . The field phasors (and the wave vector) can vary with angular frequency ω . Without loss of generality, we consider surface-wave propagation parallel to \hat{u}_x in the xy plane; i.e., $\hat{u}_y \cdot \underline{k}_\ell \equiv 0$.

Assuming an $\exp(-i\omega t)$ time-dependence, the Maxwell curl postulates yield

$$\left. \begin{aligned} \underline{k}_\ell \times \underline{\mathcal{E}}_\ell - \omega (-i\sqrt{\varepsilon_0\mu_0}\xi_\ell \underline{\mathcal{E}}_\ell + \mu_0\mu_\ell \underline{\mathcal{H}}_\ell) &= \underline{0} \\ \underline{k}_\ell \times \underline{\mathcal{H}}_\ell + \omega (\varepsilon_0\varepsilon_\ell \underline{\mathcal{E}}_\ell + i\sqrt{\varepsilon_0\mu_0}\xi_\ell \underline{\mathcal{H}}_\ell) &= \underline{0} \end{aligned} \right\}, \quad (4)$$

with $\ell = \mathcal{A}$ for half-space $z > 0$ and $\ell = \mathcal{B}$ for half-space $z < 0$. The wave vector

$$\underline{k}_\ell \equiv \left\{ \begin{array}{ll} k_{\mathcal{A}} = k_0 (q \hat{u}_x + i\alpha_{\mathcal{A}} \hat{u}_z), & z \geq 0 \\ k_{\mathcal{B}} = k_0 (q \hat{u}_x - i\alpha_{\mathcal{B}} \hat{u}_z), & z \leq 0 \end{array} \right., \quad (5)$$

with $\text{Re}\{\alpha_\ell\} > 0$ ($\ell \in \{\mathcal{A}, \mathcal{B}\}$) for surface-wave propagation. On combining Eqs. (4) and Eq. (5), a bi-quadratic dispersion relation emerges for α_ℓ ($\ell \in \{\mathcal{A}, \mathcal{B}\}$). The two α_ℓ roots with non-negative real parts are identified as

$$\left. \begin{aligned} \alpha_{\ell 1} &= \sqrt{q^2 - \kappa_{\ell R}^2} \\ \alpha_{\ell 2} &= \sqrt{q^2 - \kappa_{\ell L}^2} \end{aligned} \right\}, \quad (6)$$

with the complex-valued scalars

$$\left. \begin{aligned} \kappa_{\ell R} &= \sqrt{\varepsilon_\ell \mu_\ell} + \xi_\ell \\ \kappa_{\ell L} &= \sqrt{\varepsilon_\ell \mu_\ell} - \xi_\ell \end{aligned} \right\} \quad (7)$$

being associated with the relative wavenumbers for right and left circularly-polarized light, respectively, in an unbounded chiral medium [16]. Accordingly the field-phasor amplitudes are given as

$$\left. \begin{aligned} \underline{\mathcal{E}}_\ell &= C_{\ell 1} \underline{\mathcal{E}}_{\ell 1} + C_{\ell 2} \underline{\mathcal{E}}_{\ell 2} \\ \underline{\mathcal{H}}_\ell &= \sqrt{\frac{\varepsilon_0}{\mu_0}} \sqrt{\frac{\varepsilon_\ell}{\mu_\ell}} (C_{\ell 1} \underline{\mathcal{H}}_{\ell 1} + C_{\ell 2} \underline{\mathcal{H}}_{\ell 2}) \end{aligned} \right\}, \quad \ell \in \{\mathcal{A}, \mathcal{B}\}, \quad (8)$$

where the vectors

$$\left. \begin{aligned} \underline{\mathcal{E}}_{\mathcal{A}1} &= \alpha_{\mathcal{A}1} \hat{u}_x + \kappa_{\mathcal{A}R} \hat{u}_y + iq \hat{u}_z \\ \underline{\mathcal{E}}_{\mathcal{A}2} &= -\alpha_{\mathcal{A}2} \hat{u}_x + \kappa_{\mathcal{A}L} \hat{u}_y - iq \hat{u}_z \\ \underline{\mathcal{H}}_{\mathcal{A}1} &= -i\alpha_{\mathcal{A}1} \hat{u}_x - i\kappa_{\mathcal{A}R} \hat{u}_y + q \hat{u}_z \\ \underline{\mathcal{H}}_{\mathcal{A}2} &= -i\alpha_{\mathcal{A}2} \hat{u}_x + i\kappa_{\mathcal{A}L} \hat{u}_y + q \hat{u}_z \end{aligned} \right\} \quad (9)$$

and

$$\left. \begin{aligned} \underline{\mathcal{E}}_{\mathcal{B}1} &= -\alpha_{\mathcal{B}1} \hat{u}_x + \kappa_{\mathcal{B}R} \hat{u}_y + iq \hat{u}_z \\ \underline{\mathcal{E}}_{\mathcal{B}2} &= \alpha_{\mathcal{B}2} \hat{u}_x + \kappa_{\mathcal{B}L} \hat{u}_y - iq \hat{u}_z \\ \underline{\mathcal{H}}_{\mathcal{B}1} &= i\alpha_{\mathcal{B}1} \hat{u}_x - i\kappa_{\mathcal{B}R} \hat{u}_y + q \hat{u}_z \\ \underline{\mathcal{H}}_{\mathcal{B}2} &= i\alpha_{\mathcal{B}2} \hat{u}_x + i\kappa_{\mathcal{B}L} \hat{u}_y + q \hat{u}_z \end{aligned} \right\}. \quad (10)$$

The four scalars $C_{\mathcal{A}1,2}$ and $C_{\mathcal{B}1,2}$ introduced in Eqs. (8), as well as the relative wavenumber q , are determined by enforcing boundary conditions across the planar interface $z = 0$, as follows. The continuity of tangential components of the electric and magnetic field phasors across the planar interface $z = 0$ imposes four conditions [25] which may be represented compactly as

$$[M] \cdot \begin{bmatrix} C_{\mathcal{A}1} \\ C_{\mathcal{A}2} \\ C_{\mathcal{B}1} \\ C_{\mathcal{B}2} \end{bmatrix} = \begin{bmatrix} 0 \\ 0 \\ 0 \\ 0 \end{bmatrix}, \quad (11)$$

wherein the 4×4 matrix

$$[M] = \begin{bmatrix} \alpha_{\mathcal{A}1} & -\alpha_{\mathcal{A}2} & \alpha_{\mathcal{B}1} & -\alpha_{\mathcal{B}2} \\ \kappa_{\mathcal{A}R} & \kappa_{\mathcal{A}L} & -\kappa_{\mathcal{B}R} & -\kappa_{\mathcal{B}L} \\ \alpha_{\mathcal{A}1}\sqrt{\frac{\varepsilon_{\mathcal{A}}}{\mu_{\mathcal{A}}}} & \alpha_{\mathcal{A}2}\sqrt{\frac{\varepsilon_{\mathcal{A}}}{\mu_{\mathcal{A}}}} & \alpha_{\mathcal{B}1}\sqrt{\frac{\varepsilon_{\mathcal{B}}}{\mu_{\mathcal{B}}}} & \alpha_{\mathcal{B}2}\sqrt{\frac{\varepsilon_{\mathcal{B}}}{\mu_{\mathcal{B}}}} \\ -\kappa_{\mathcal{A}R}\sqrt{\frac{\varepsilon_{\mathcal{A}}}{\mu_{\mathcal{A}}}} & \kappa_{\mathcal{A}L}\sqrt{\frac{\varepsilon_{\mathcal{A}}}{\mu_{\mathcal{A}}}} & \kappa_{\mathcal{B}R}\sqrt{\frac{\varepsilon_{\mathcal{B}}}{\mu_{\mathcal{B}}}} & -\kappa_{\mathcal{B}L}\sqrt{\frac{\varepsilon_{\mathcal{B}}}{\mu_{\mathcal{B}}}} \end{bmatrix}. \quad (12)$$

For a nontrivial solution to Eq. (11), the matrix $[M]$ must be singular. Hence the dispersion equation

$$\det [M] = 0 \quad (13)$$

arises, from which q may be extracted, generally by numerical means [26]. Once q is known, relative values of the four scalars $C_{\mathcal{A}1,2}$ and $C_{\mathcal{B}1,2}$ can be determined from Eq. (11) by straightforward algebraic manipulations.

3 Numerical studies

The partnering materials \mathcal{A} and \mathcal{B} are both isotropic chiral materials [16], per the Tellegen constitutive relations (1). To allow flexibility in specifying the constitutive parameters for these materials, both partnering materials \mathcal{A} and \mathcal{B} are modeled as HCMs. Specifically, partnering material $\ell \in \{\mathcal{A}, \mathcal{B}\}$ arises from the homogenization of two component materials, namely component material ℓ_a which is an achiral, nonmagnetic, isotropic material characterized by the relative permittivity ε_a^ℓ and component material ℓ_b which is an isotropic chiral material characterized by the relative constitutive parameters ε_b^ℓ , μ_b^ℓ and ξ_b^ℓ per the Tellegen constitutive relations (1). Both component materials in each half-space $z \leq 0$ are assumed to be randomly distributed as electrically small spheres, with the volume fraction of component material ℓ_a being f_a^ℓ and that of component material ℓ_b being $f_b^\ell = 1 - f_a^\ell$.

Estimates of the constitutive parameters of the partnering materials \mathcal{A} and \mathcal{B} , namely $\varepsilon^\ell, \mu^\ell$ and ξ^ℓ ($\ell \in \{\mathcal{A}, \mathcal{B}\}$), are provided by the Bruggeman homogenization formalism [22, 27]. This process involves numerically solving the following nonlinear matrix equation

$$\begin{aligned} f_a^\ell ([K_a^\ell] - [K^\ell]) \cdot \{[I] + [D^\ell] \cdot ([K_a^\ell] - [K^\ell])\}^{-1} = \\ f_b^\ell ([K^\ell] - [K_b^\ell]) \cdot \{[I] + [D^\ell] \cdot ([K_b^\ell] - [K^\ell])\}^{-1}, \end{aligned} \quad (14)$$

wherein the constitutive 2×2 matrixes

$$\left. \begin{aligned} [K_a^\ell] &= \begin{bmatrix} \varepsilon_a^\ell & 0 \\ 0 & 1 \end{bmatrix} \\ [K_b^\ell] &= \begin{bmatrix} \varepsilon_b^\ell & i\xi_b^\ell \\ -i\xi_b^\ell & \mu_b^\ell \end{bmatrix} \\ [K^\ell] &= \begin{bmatrix} \varepsilon^\ell & i\xi^\ell \\ -i\xi^\ell & \mu^\ell \end{bmatrix} \end{aligned} \right\}, \quad (15)$$

the depolarization 2×2 matrix

$$[D^\ell] = \frac{1}{3[\varepsilon^\ell\mu^\ell + (\xi^\ell)^2]} \begin{bmatrix} \mu^\ell & -\xi^\ell \\ \xi^\ell & \varepsilon^\ell \end{bmatrix}, \quad (16)$$

and $[I]$ is the 2×2 identity matrix.

For the isotropic chiral component material, for both partnering materials \mathcal{A} and \mathcal{B} , we fixed $\varepsilon_b^\mathcal{A} \equiv \varepsilon_b^\mathcal{B} = 3 + 0.01i$, $\mu_b^\mathcal{A} \equiv \mu_b^\mathcal{B} = 0.95 + 0.0002i$, and $\xi_b^\mathcal{A} \equiv \xi_b^\mathcal{B} = 0.1 + 0.001i$, these values being consistent with

certain mildly dissipative, isotropic chiral metamaterials [28]. For the isotropic achiral component material for partnering material \mathcal{A} , we fixed $\varepsilon_a^{\mathcal{A}} = 2 - 0.02i$. Thus, the component material \mathcal{A}_a is an active material. The selected value of $\varepsilon_a^{\mathcal{A}}$ falls within the range commonly used for active components of metamaterials in the visible regime. For example, a mixture of Rhodamine 800 and Rhodamine 6G, yields a relative permittivity with real part in the range (1.8, 2.3) and imaginary part in the range (-0.15, -0.02) for the frequency range 440–500 THz, depending upon the relative concentrations and the external pumping rate [29]. The volume fraction of component material \mathcal{A}_a was fixed at $f_a^{\mathcal{A}} = 0.3$. Consequently, the Bruggeman equation (14) delivers the constitutive parameter estimates $\varepsilon^{\mathcal{A}} = 2.6721 - 0.0007i$, $\mu^{\mathcal{A}} = 0.9645 + 0.0001$, and $\xi^{\mathcal{A}} = 0.0675 + 0.0006i$. Hence, partnering material \mathcal{A} is an isotropic chiral material that simultaneously supports amplification and attenuation of plane waves, depending upon the state of circular polarization [23]. Several manifestations of simultaneous amplification and attenuation of plane waves have been reported recently [30], including within the context of surface waves [31, 32].

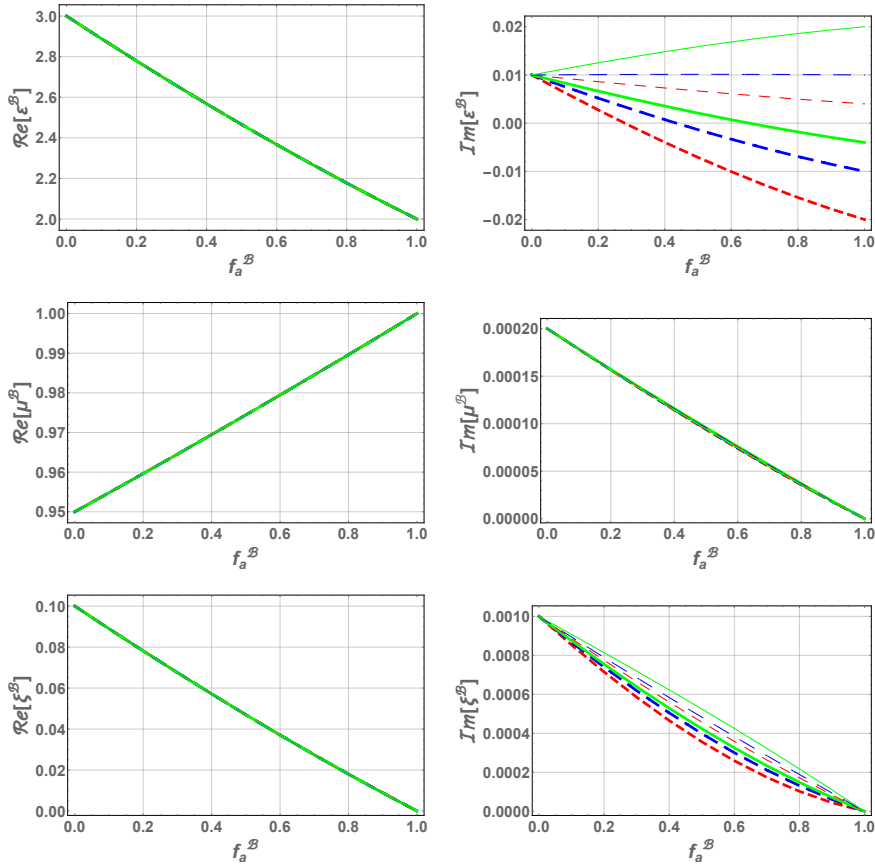


Figure 1: Bruggeman estimates of the real and imaginary parts of the relative constitutive parameters $\varepsilon^{\mathcal{B}}$, $\mu^{\mathcal{B}}$, and $\xi^{\mathcal{B}}$ plotted against volume fraction $f_a^{\mathcal{B}}$ for $\varepsilon_a^{\mathcal{B}} = 2 - 0.02di$. Key: $d = 1.0$ (thick dashed red curve), 0.5 (thick broken dashed blue curve), 0.2 (thick solid green curve), -0.2 (thin dashed red curve), -0.5 (thin broken dashed blue curve), and -1.0 (thin solid green curve).

We begin our presentation of numerical results with the case where the achiral component material \mathcal{B}_a is specified by the relative permittivity $\varepsilon_a^{\mathcal{B}} = 2 - 0.02di$. Let us consider $d \in \{-0.2, -0.5, -1\}$ for which component material \mathcal{B}_a is a weakly dissipative dielectric material and $d \in \{0.2, 0.5, 1\}$ for which component material \mathcal{B}_a is an active dielectric material. Estimates of the relative constitutive parameters of partnering material \mathcal{B} , as provided by the Bruggeman equation (14), are plotted as functions of volume fraction $f_a^{\mathcal{B}}$

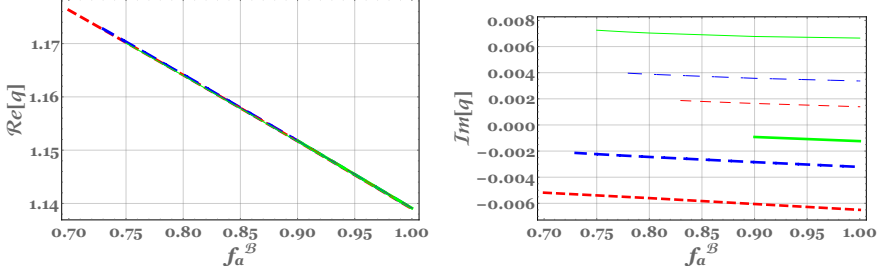


Figure 2: Real and imaginary parts of the relative wavenumber q plotted against volume fraction f_a^B for $\varepsilon_a^B = 2 - 0.02di$. Key: $d = 1.0$ (thick dashed red curve), 0.5 (thick broken dashed blue curve), 0.2 (thick solid green curve), -0.2 (thin dashed red curve), -0.5 (thin broken dashed blue curve), and -1.0 (thin solid green curve).

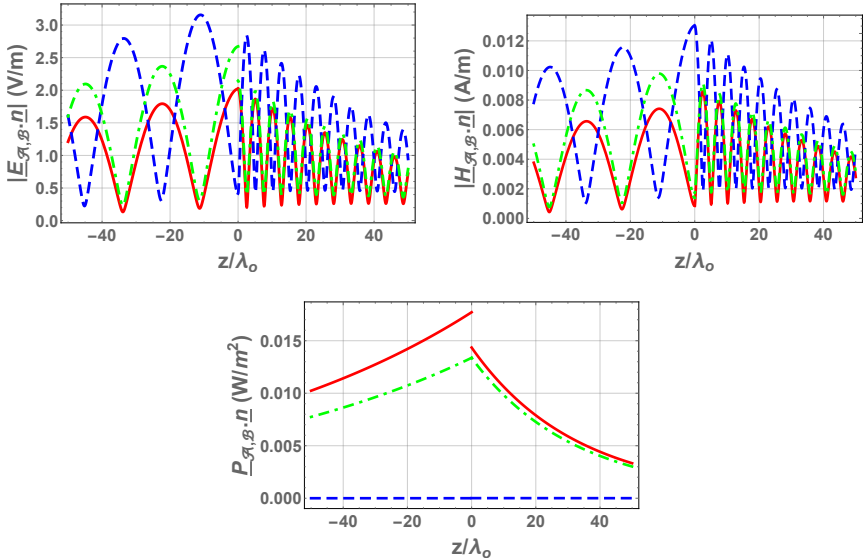


Figure 3: Magnitudes of $E_{A,B}(z\hat{u}_z) \cdot \underline{n}$, and $H_{A,B}(z\hat{u}_z) \cdot \underline{n}$, along with $P_{A,B}(z\hat{u}_z) \cdot \underline{n}$, plotted versus z/λ_0 , when $\varepsilon_a^B = 2 - 0.02di$, $f_a^B = 0.85$, $d = 0.5$, and $C_{A1} = 1 \text{ V m}^{-1}$. Key: $\underline{n} = \hat{u}_x$ solid red curves; $\underline{n} = \hat{u}_y$ dashed blue curves; $\underline{n} = \hat{u}_z$ broken dashed curves.

in Fig. 1. The real parts of ε^B , μ^B , and ξ^B are almost independent of the parameter d ; they vary in an approximately linear manner as f_a^B varies. The imaginary part of ε^B is negative valued for $d > 0$ and positive valued for $d < 0$. And the magnitude $|\text{Im}\{\varepsilon^B\}|$ is larger when the magnitude of d is larger. The imaginary parts of μ^B and ξ^B are both much less sensitive to d than is $\text{Im}\{\varepsilon^B\}$; both are positive valued for all values of d and both decay to zero in the limit $f_a^B \rightarrow 1$.

For $d \in \{-1, -0.5, -0.2, 0.2, 0.5, 1\}$, a surface wave is supported for certain ranges of volume fraction f_a^B . The real and imaginary parts of the relative wavenumber q for these surface waves are plotted against f_a^B in Fig. 2. The volume fraction ranges of that support surface waves are as follows: $f_a^B \in (0.75, 1]$ for $d = -1$, $f_a^B \in (0.78, 1]$ for $d = -0.5$, $f_a^B \in (0.83, 1]$ for $d = -0.2$, $f_a^B \in (0.90, 1]$ for $d = 0.2$, $f_a^B \in (0.73, 1]$ for $d = 0.5$, and $f_a^B \in (0.70, 1]$ for $d = 1$. Notably, surface waves are not supported at all for small values of f_a^B . The real parts of q decrease approximately linearly as f_a^B increases, and these values are almost independent of d . The imaginary parts of q decrease slightly as f_a^B increases, with the magnitude $|\text{Im}\{q\}|$ being greater

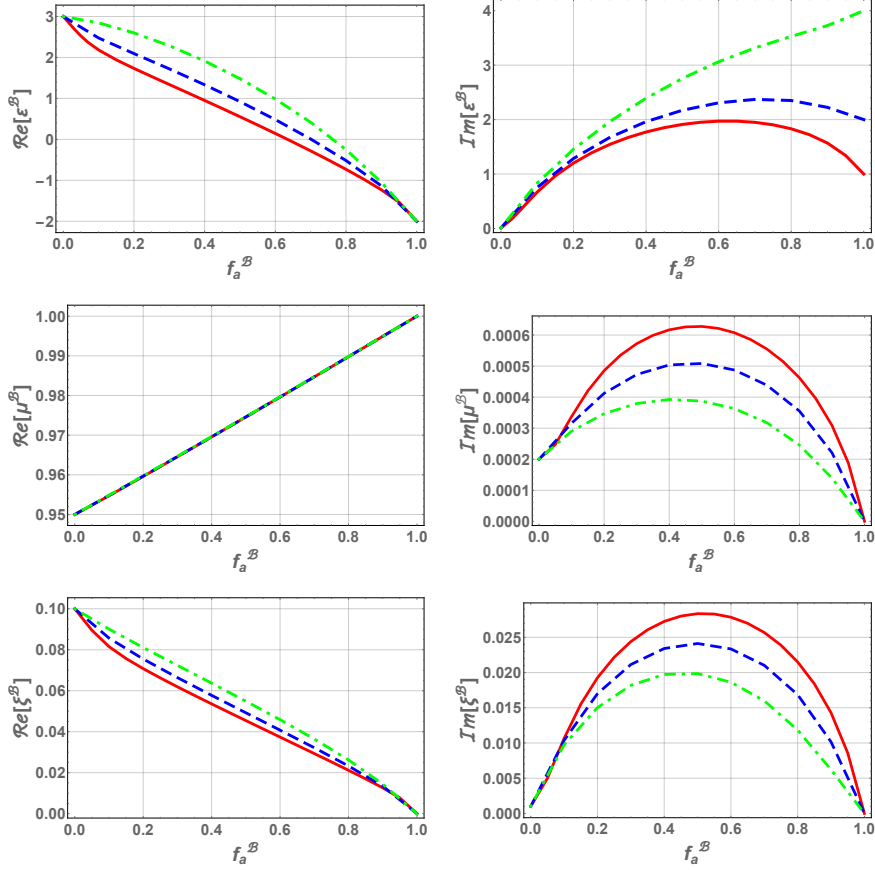


Figure 4: Bruggeman estimates of the real and imaginary parts of the relative constitutive parameters ε^B , μ^B , and ξ^B plotted against volume fraction f_a^B for $\varepsilon_a^B = -2 + 0.02di$. Key: $d = 50$ (solid red curve), 100 (dashed blue curve), and 200 (broken dashed green curve).

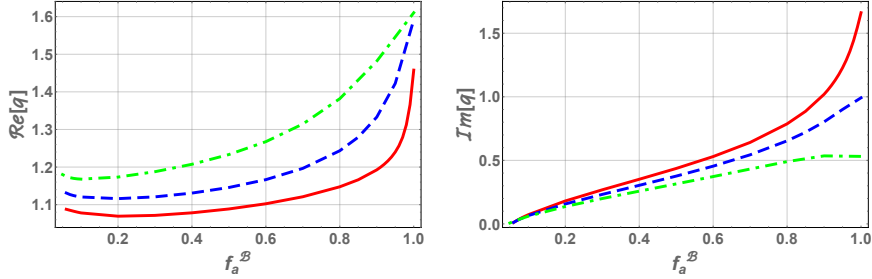


Figure 5: Real and imaginary parts of the relative wavenumber q plotted against volume fraction f_a^B for $\varepsilon_a^B = -2 + 0.02di$. Key: $d = 50$ (solid red curve), 100 (dashed blue curve), and 200 (broken dashed green curve).

when the magnitude of d is greater. Also $\operatorname{Im}\{q\} > 0$ when $d < 0$ and $\operatorname{Im}\{q\} < 0$ when $d > 0$; that is, the surface wave attenuates in the direction of propagation when the component material \mathcal{B}_a is dissipative and the surface wave is amplified in the direction of propagation when the component material \mathcal{B}_a is active.

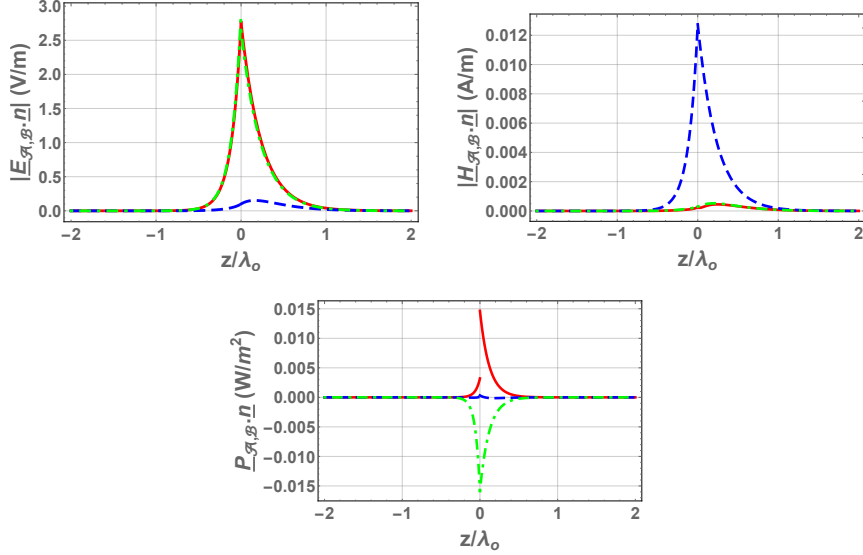


Figure 6: Magnitudes of $\underline{E}_{\mathcal{A},\mathcal{B}}(z\hat{u}_z) \cdot \underline{n}$, and $\underline{H}_{\mathcal{A},\mathcal{B}}(z\hat{u}_z) \cdot \underline{n}$, along with $\underline{P}_{\mathcal{A},\mathcal{B}}(z\hat{u}_z) \cdot \underline{n}$, plotted versus z/λ_0 , when $\varepsilon_a^{\mathcal{B}} = -2 + 0.02di$, $f_a^{\mathcal{B}} = 0.85$, $d = 100$, and $C_{\mathcal{A}1} = 1 \text{ V m}^{-1}$. Key: $\underline{n} = \hat{u}_x$ solid red curves; $\underline{n} = \hat{u}_y$ dashed blue curves; $\underline{n} = \hat{u}_z$ broken dashed curves.

Further illumination on the nature of these surface waves is offered in Fig. 3 wherein profiles of the electric and magnetic field phasors are provided. Specifically, plotted are $|\underline{E}_\ell(z\hat{u}_z) \cdot \underline{n}|$ and $|\underline{H}_\ell(z\hat{u}_z) \cdot \underline{n}|$, $\ell \in \{\mathcal{A}, \mathcal{B}\}$, versus z/λ_0 for $\underline{n} \in \{\hat{u}_x, \hat{u}_y, \hat{u}_z\}$, when $d = 0.5$ and $f_a^{\mathcal{B}} = 0.85$, with $C_{\mathcal{A}1} = 1 \text{ V m}^{-1}$. Also plotted are the corresponding profiles of the Cartesian components $\underline{P}_\ell(z\hat{u}_z) \cdot \underline{n}$, $\ell \in \{\mathcal{A}, \mathcal{B}\}$ and $\underline{n} \in \{\hat{u}_x, \hat{u}_y, \hat{u}_z\}$, of the time-averaged Poynting vector [25]

$$\underline{P}_\ell(\underline{r}) = \frac{1}{2} \text{Re} [\underline{E}_\ell(\underline{r}) \times \underline{H}_\ell^*(\underline{r})], \quad \ell \in \{\mathcal{A}, \mathcal{B}\}, \quad (17)$$

where the asterisk denotes the complex conjugate. The surface wave is rather loosely localized to the planar interface $z = 0$, with significant spreading of the fields into both the half-spaces $z > 0$ and $z < 0$ even at $z = \pm 40\lambda_0$. The surface wave is a little more tightly bound to the planar interface $z = 0$ in the half-space $z > 0$ than in the half-space $z < 0$. Profiles of the field phasors are qualitatively similar for the other values of d considered here.

Next let us explore the case where the achiral component material \mathcal{B}_a is a plasmonic material. To this end, we select the relative permittivity $\varepsilon_a^{\mathcal{B}} = -2 + 0.02di$ with $d \in \{50, 100, 200\}$. In Fig. 4 estimates of the relative constitutive parameters of partnering material \mathcal{B} , as provided by the Bruggeman equation (14), are plotted as functions of volume fraction $f_a^{\mathcal{B}}$. The real parts of $\varepsilon^{\mathcal{B}}$ and $\xi^{\mathcal{B}}$ are generally larger when the parameter d is larger, especially for mid-range values of $f_a^{\mathcal{B}}$, whereas the real part of $\mu^{\mathcal{B}}$ is almost independent of d . The imaginary part of $\varepsilon^{\mathcal{B}}$ is larger for larger values of d . In contrast, the imaginary parts of $\mu^{\mathcal{B}}$ and $\xi^{\mathcal{B}}$ are larger for smaller values of d and these quantities both decay to zero in the limit $f_a^{\mathcal{B}} \rightarrow 1$.

With the plasmonic component material \mathcal{B}_a and $d \in \{50, 100, 200\}$, a surface wave is supported for wide ranges of volume fraction $f_a^{\mathcal{B}}$, but not for all values of $f_a^{\mathcal{B}}$. The real and imaginary parts of the relative wavenumber q for these surface waves are plotted against $f_a^{\mathcal{B}}$ in Fig. 5. Surface waves are supported for the following ranges of volume fraction: $f_a^{\mathcal{B}} \in (0.06, 1]$ for $d = 50$, $f_a^{\mathcal{B}} \in (0.06, 1]$ for $d = 100$, and $f_a^{\mathcal{B}} \in (0.05, 1]$ for $d = 200$. Notably, surface waves are not supported in the limit $f_a^{\mathcal{B}} \rightarrow 0$. The real parts of q increase quite sharply as $f_a^{\mathcal{B}}$ increases, depending upon the value d . Likewise, the imaginary parts of q increase as $f_a^{\mathcal{B}}$ increases, with the largest values of $\text{Im}\{q\}$ arising when the magnitude of d is smallest. Also, for all values of d , $\text{Im}\{q\} > 0$ which indicates that the surface waves are attenuated in the direction of propagation.

Profiles of the electric and magnetic field phasors are presented in Fig. 6, for the case where component material \mathcal{B}_a is a plasmonic material, in order to shed further light on the nature of these surface waves. For these computations, $d = 100$ and $f_a^{\mathcal{B}} = 0.85$, with $C_{A1} = 1 \text{ V m}^{-1}$. Also plotted are the corresponding profiles of the Cartesian components of the time-averaged Poynting vector. The surface wave is quite tightly localized to the planar interface $z = 0$, much more so than the corresponding surface wave represented in Fig. 3, with the surface wave being essentially confined to the region $-\lambda_0 < z < \lambda_0$. The surface wave is rather more tightly bound to the planar interface $z = 0$ in the half-space $z < 0$ than in the half-space $z > 0$. Profiles of the field phasors are qualitatively similar for the other values of d considered here.

4 Closing remarks

The planar interface of two isotropic chiral materials has been shown to support surface-wave propagation for certain constitutive parameter ranges. When the component material \mathcal{B}_a is a plasmonic material the surface waves are akin to SPP waves. But when the component material \mathcal{B}_a is a dielectric material the surface wave is not akin to a SPP wave, since $\text{Re}\{\varepsilon^A\} > 0$ and $\text{Re}\{\varepsilon^B\} > 0$. Furthermore when the component material \mathcal{B}_a is a dielectric material the surface wave is not akin to a Dyakonov wave, since both partnering materials are isotropic. These surface waves are not akin to any of the well-established types of surface wave [1].

Notably, for all surface-wave solutions reported herein the constitutive parameters of the partnering materials are complex-valued with non-zero imaginary parts. The question arises: Is surface-wave propagation possible for the idealized case in which the constitutive parameters of the partnering materials are real-valued? Owing to the intractability of the dispersion equation (13), a definitive answer is not available. However, extensive numerical searches were undertaken in an attempt to find surface-wave solutions for real-valued constitutive parameters but none were found. Therefore, our numerical evidence suggests that the answer to this question is ‘no’.

Acknowledgments. MN acknowledges the support of the Higher Education Commission (HEC) of Pakistan for a six-month research visit to the University of Edinburgh via grant number HRD-2018-8668.

References

- [1] J.A. Polo Jr., T.G. Mackay, and A. Lakhtakia, *Electromagnetic Surface Waves: A Modern Perspective* (Elsevier, 2013).
- [2] J.M. Pitarke, V.M. Silkin, E.V. Chulkov, and P.M. Echenique, “Theory of surface plasmon and surface-plasmon polaritons,” *Rep. Prog. Phys.* **70**, 1–87 (2007).
- [3] S.A. Maier, *Plasmonics: Fundamentals and Applications* (Springer, 2007).
- [4] Z. Jacob and E.E. Narimanov, “Optical hyperspace for plasmons: Dyakonov states in metamaterials,” *Appl. Phys. Lett.* **93**, 221109 (2008).
- [5] J. Homola (Ed.), *Surface Plasmon Resonance Based Sensors* (Springer, 2006).
- [6] I. Abdulhalim, M. Zourob, and A. Lakhtakia, “Surface plasmon resonance for biosensing: A mini-review,” *Electromagnetics* **28**, 214–242 (2008).
- [7] F.N. Marchevskii, V.L. Strizhevskii, and S.V. Strizhevskii, “Singular electromagnetic waves in bounded anisotropic media,” *Sov. Phys. Solid State* **26**, 911–912 (1984).
- [8] M.I. D'yakonov, “New type of electromagnetic wave propagating at an interface,” *Sov. Phys. JETP* **67**, 714–716 (1988).
- [9] D.B. Walker, E.N. Glytsis, and T.K. Gaylord, “Surface mode at isotropic-uniaxial and isotropic-biaxial interfaces,” *J. Opt. Soc. Am. A* **15**, 248–260 (1998).

[10] O. Takayama, L. Crasovan, D. Artigas, and L. Torner, “Observation of Dyakonov surface waves,” *Phys. Rev. Lett.* **102**, 043903 (2009).

[11] O. Takayama, L.-C. Crasovan, S.K. Johansen, D. Mihalache, D. Artigas, and L. Torner, “Dyakonov surface waves: A review,” *Electromagnetics* **28**, 126–145 (2008).

[12] T.G. Mackay and A. Lakhtakia, “Temperature-mediated transition from Dyakonov surface waves to surface-plasmon-polariton waves,” *IEEE Photon. J.* **8**, 4802813 (2016).

[13] M. Faryad and F. Abbas, “On the Dyakonov waves guided by the interface with a columnar thin film,” 12th International Congress on Artificial Materials for Novel Wave Phenomena - Metamaterials 2018 Espoo, Finland, Aug. 27th - Sept. 1st (2018).

[14] O. Takayama, E. Shkondin, A. Bodganov, M. Esmail Aryae Panah, K. Golenitskii, P. Dmitriev, T. Repan, R. Malureanu, P. Belov, F. Jensen, and A.V. Lavrinenko, “Midinfrared surface waves on a high aspect ratio nanotrench platform,” *ACS Photonics* **4**, 2899–2907 (2017).

[15] P. Li, I. Dolado, F.J. Alfaro-Mozaz, F. Casanova, L.E. Hueso, S. Liu, J.H. Edgar, A.Y. Nikitin, S. Vélez, and R. Hillenbrand, Infrared hyperbolic metasurface based on nanostructured van der Waals materials, *Science* **359**, 892–896 (2018).

[16] A. Lakhtakia, *Beltrami Fields in Chiral Media* (World Scientific, 1994).

[17] D.N. Pattanayak and J.L. Birman, “Wave propagation in optically active and magnetoelectric media of arbitrary geometry,” *Phys. Rev. B* **24**, 4271–4278 (1981).

[18] N. Engheta and P. Pelet, Surface waves in chiral layers. *Opt. Lett.* **16**, 723–725 (1991).

[19] A.N. Fantino, “Planar interface between a chiral medium and a metal: surface wave excitation,” *J. Mod. Opt.* **43**, 2581–2593 (1996).

[20] G. Pellegrini, M. Finazzi, M. Celebrano, L. Duò, and P. Biagioni, “Chiral surface waves for enhanced circular dichroism,” *Phys. Rev. B* **95**, 241402(R) (2017).

[21] J. Noonan and T.G. Mackay, “On electromagnetic surface waves supported by an isotropic chiral material,” *Opt. Commun.* **434**, 224–229 (2019).

[22] T.G. Mackay and A. Lakhtakia, *Modern Analytical Electromagnetic Homogenization* (Morgan & Claypool, 2015).

[23] T.G. Mackay and A. Lakhtakia, “Simultaneous amplification and attenuation in isotropic chiral materials,” *J. Opt. (UK)* **18**, 055104 (2016).

[24] B.Y.-K. Hu, “Kramers–Kronig in two lines,” *Am. J. Phys.* **57**, 821 (1989).

[25] H.C. Chen, *Theory of Electromagnetic Waves* (McGraw–Hill, 1983).

[26] Y. Jaluria, *Computer Methods for Engineering* (Taylor & Francis, 1996).

[27] R. D. Kampia and A. Lakhtakia, “Bruggeman model for chiral particulate composites,” *J. Phys. D: Appl. Phys.* **25**, 1390–1394 (1992).

[28] D.-H. Kwon, D.H. Werner, A.V. Kildishev, and V.M. Shalaev, “Material parameter retrieval procedure for general bi-isotropic metamaterials and its application to optical chiral negative-index metamaterial design,” *Opt. Exp.* **16**, 11822–11829 (2008).

[29] L. Sun, X. Yang, and J. Gao, “Loss-compensated broadband epsilon-near-zero metamaterials with gain media,” *Appl. Phys. Lett.* **103**, 201109 (2013).

- [30] T.G. Mackay and A. Lakhtakia, “Dynamically controllable anisotropic metamaterials with simultaneous attenuation and amplification,” *Phys. Rev. A* **92**, 053847 (2015).
- [31] T.G. Mackay and A. Lakhtakia, “Simultaneous existence of amplified and attenuated surface-plasmon-polariton waves,” *J. Opt. (India)* **47**, 527–533 (2018) .
- [32] T.G. Mackay and A. Lakhtakia, “Simultaneous existence of amplified and attenuated Dyakonov surface waves,” *Opt. Commun.* **427**, 175–179 (2018).